# A novel plied yarn structure with negative Poisson's ratio

Zhaoyang Ge[a, b], Hong Hu[a*], Shirui Liu[a]

[a] Institute of Textiles and Clothing, The Hong Kong Polytechnic University, Hung Hom, Kowloon, Hong Kong; [b] Henan Key Laboratory of Functional Textile Materials, Zhongyuan University of Technology, Zhengzhou, People's Republic of China

**Abstract**

This paper presents an experimental and geometrical study of a novel kind of plied yarn structure with negative Poisson's ratio (NPR). The deformation mechanism of the yarn structure formed with two stiff yarns and two soft yarns to achieve NPR behavior was firstly introduced. Based on the proposed yarn structure, four kinds of yarn samples were then fabricated with two kinds of stiff yarns and two types of soft yarns and tested under the axial extension to verify their auxetic or NPR effect. A geometric analysis was finally conducted to theoretically calculate the Poisson's ratio of the yarn structure and compared with the experimental results. The study shows that the proposed yarn structure has obvious NPR effect and the geometrical analysis can well predict its Poisson's ratio in the higher axial strain range. It is expected that this study could promote further development of auxetic textiles with unusual behavior.

**Keywords**: plied yarn structure, negative Poisson's ratio, deformation mechanism, geometrical analysis

## 1. Introduction

Materials with negative Poisson's ratio (NPR) are known as auxetic materials. Different from most conventional materials with positive Poisson's ratio, auxetic materials laterally expand in tension or laterally contract in compression (Liu & Hu, 2010). This counterintuitive behavior leads to a lot of interesting properties such as the formation of synclastic curvatures under bending, effective de-coupling of the Young's and shear moduli, enhanced energy absorption ability and indentation resistance (Liu & Hu, 2010). In the past two and half decades, many auxetic materials, both natural and man-made, have been widely investigated, including polymeric foams (Lakes, 1987; Chan & Evans, 1997), honeycomb structures (Masters& Evans, 1996), polyethylene (Alderson & Evans, 1992), skins (Lees, Vincent & Hillerton, 1991), zeolites (Grima, Gatt, Zammit, Williams, Alderson & Walton, 2007), single crystal arsenic (Gunton, & Saunders, 1972), and composites (Evans, Donoghue, & Alder, 2004), etc.

The study of auxetic materials based on textile structures has attracted a great attention in recent years (Evans, Donoghue, & Alder, 2004; Wang & Hu, 2014). Auxetic textiles include auxetic fibers (Alderson, Alderso, Smart, Simkins, & Davi, 2002; Ravirala, Alderson, Davies, Simkins, & Alderson, 2006), auxetic yarns (Hook, 2011; Evans, Sloan, Wright & Burns, 2010; Lee, Lee, Koh & Heo, 2011) and auxetic fabrics (Wang, Hu & Xiao 2014; Ge, Hu & Liu 2013; Wang & Hu, 2014; Ge & Hu, 2013; Alderson, Alderson, Anand, Simkins, Nazare & Ravirala, 2012; Hu, Wang & Liu, 2011; Liu, Hu, Lam & Liu, 2010; Ugbolue, Kim, Warner, Fan, Yang, Kyzymchuk, Feng & Lord, 2011; Ugbolue, Kim, Warner, Fan, Yang, Kyzymchuk, Feng, & Lord, 2011). Among various auxetic textile materials which have been developed up to now, helical auxetic yarn structure (Hook, 2011) invented by Hook Patrick has demonstrated a great interest for practical applications. The helical auxetic yarn structure is constructed by combining two yarn components with different stiffness in a double-helix

geometry, in which a relatively stiffer yarn, referred as a “wrap”, is helically wound around a more compliant and initially straight elastomeric cylinder, referred as a “core’. Several studies on this kind of auxetic yarn structure have been conducted. Sloan et al. carried out an experimental study on helical auxetic yarn made of monofilaments (Sloan, Wright & Evans, 2011), and demonstrated that the starting wrap angle of the yarn has the greatest effect on auxetic behavior both in terms of the magnitude and strain range over which it may be observed. Wright et al. performed a numerical study on the tensile properties of helical auxetic yarn using finite element method (Wright, Sloan & Evans, 2010). According to their study, the stiffness of the component fibers and the initial helical wrap angle are critical design parameters, and strain-dependent changes in cross section must be taken into consideration during the analysis. Wright et al. also investigated pore opening effect of woven fabrics made of auxetic yarn (Wright, Burns, James, Sloan & Evans, 2011). This behavior makes auxetic yarn very attractive for some special applications, such as filtration in which pore opening size of filter can be controlled by tension (Lakes, 1987; Alderson, Rasburn, Ameer-Beg, Mullarkey, Perrie, Evans, 2000), bomb blast curtains which can open a large number of pores under tension allowing the shock wave through but leaving the curtains intact to catch glass and other debris (Hook, 2011), smart bandage in which applied drugs can be automatically delivered (Alderson, A.; Alderson, K. 2005), etc. Bhattacharya et al. recently studied the effect of the interaction between the core and the wrap fiber on the auxetic behavior of the helical yarn, including the effect of their relative moduli, and found that an elevated difference in component moduli causes the wrap fiber embedding itself into the core fiber, thus decreasing the auxetic effect (Bhattacharya, Zhang, Ghita & Evans, 2014). Lim explored a variant of the auxetic helical yarn by sewing an inextensible thin cord through an elastic fat cord. When the semi-auxetic yarn is stretched in the longitudinal direction, it exhibits conventional and auxetic behavior in the plane perpendicular and parallel, respectively (Lim, 2014). In addition to helical auxetic yarn structure and its made fabrics,

composites reinforced by auxetic yarn made of carbon fiber (Miller, Hook, Smith, Wang & Evans, 2009) and woven fabric made of auxetic yarn (Miller, Ren, Smith & Evans, 2012) were also investigated by Miller et al. Their studies demonstrated that such composites exhibit auxetic behavior as well. Helical auxetic yarns made of optical fiber used as sensors (Hook, 2009) and moisture sensitive auxetic material for functional garment( Lee, Lee, Koh & Heo, 2011) were also suggested by Hook and Lee et al., respectively. Although a number of applications can be explored using the helical auxetic yarns, some intrinsic structural drawbacks could be found. The first drawback is that the stiff wrap can easily slip along the surface of the core yarn, resulting in the difficulty to make very regular yarn in twist. The second one is its low yarn structural stability since the stiff wrap can easily get loose after extension.

The present work aims to study a novel kind of auxetic plied yarn structure formed with two different kinds of yarn components to overcome the above drawbacks. Compared to the existing helical auxetic yarn structure, the twist of the newly proposed auxetic yarn would be easier controlled, so that the twist regularity of the auxetic yarn could be improved. For understanding the mechanism to realize the auxetic effect of the yarn structure, both experimental and geometrical analyses were conducted. Four different kinds of samples were fabricated with two types of stiff yarns and two types of soft yarns and tested under axial tensile condition to examine their auxetic effect. The geometrical analysis was conducted to theoretically calculate the Poisson's ratio values of the auxetic plied yarn structure for any given tensile strain. It is expected that this study could promote further development of auxetic textiles with unusual properties.

## 2. Structure and deformation mechanism

The novel auxetic plied yarn structure is schematically illustrated in Figure 1 (a). It consists of two soft yarns and two stiff yarns with different diameters (Hu & Liu, 2013). Two kinds of

yarn components are alternately placed along the axial direction of the auxetic plied yarn structure and twisted together. Compared to the existing helical auxetic yarn structure, the twist of the novel yarn can be easier controlled, so that the twist regularity of the auxetic plied yarn can be improved.

The deformation mechanism of the structure under the axial extension is schematically represented in Figure 1 (b), from which it can be seen how auxetic behavior is achieved. At the initial state (Figure 1(b)-1), two stiff yarns are located outside the two soft yarns. At this state, all the yarn components are tightly contacted along their lateral surface in a helical form. As shown in Figure 1(b)-2, when the auxetic composite yarn structure is stretched along its axial direction, two stiff yarn components which have relatively lower axial deformation will tend to migrate into the inside of the auxetic composite yarn structure. This migration will push the soft yarns out and thus leading to an increase of the cross-sectional size of auxetic plied yarn structure. As a result, auxetic effect is achieved. Figure 1(b)-3 shows the full moving-in of the stiff yarns into the center of the auxetic composite yarn structure. At this state, the auxetic plied yarn structure reaches its maximum cross sectional size and the two stiff yarns get contacted each other. As shown in Figure 1(b)-4, if the auxetic plied yarn continues to be stretched, the diameters of both soft and stiff yarns will start to decrease due to increased tension. At this state, although the cross-sectional size of the auxetic plied yarn structure starts to reduce, it is still bigger than that at the initial state. So the auxetic plied yarn structure still has auxetic effect. Once the auxetic yarn structure is relieved from tension before breakage, both the soft and stiff yarn components can easily return to their initial position due to their elasticity.

## 3. Experimental

### *3.1 Fabrication of auxetic yarn samples*

In order to examine auxetic behavior of the novel auxetic plied yarn structure, four kinds of yarn samples were fabricated with two types of stiff yarns and two types of soft yarns using a specially built-up prototype. As shown in Figure 2, the manufacturing process of the auxetic plied yarn structure includes three steps. In the first step, two soft yarns and two stiff yarns are alternately arranged and fed from the bobbins fixed onto a rotating circular disc to the working area of the prototype. In the second step, the fed yarns are twisted together by rotating the circular disc and the auxetic plied yarn structure is formed at point A. The twist of yarn can be adjusted by changing the rotation speed of the rotating disc and the taking-up speed of the auxetic yarn. In the third step, the twisted yarn is taken away from the working area and is wound on a bobbin. As important processing parameters, the twist and yarn tension were carefully controlled during the manufacturing process to assure the quality of the yarns. The four types of auxetic yarns fabricated are shown in Figure 3 and their yarn components and structural parameters are listed in Table 1.

### *3.2 Tensile testing and calculation of Poisson's ratio*

The above four kinds of auxetic plied yarn samples were subjected to a tensile test along their axial direction until breakage of the stiff yarns using an INSTRON 5566 tester (Instron Worldwide Headquarters, Norwood, Massachusetts, USA). The set-up of the testing system is shown in Figure 4. The gauge distance and tensile speed were set as 250 mm and 50 mm/min, respectively. In order to calculate the radial strain of the auxetic plied structure for any given axial strain, a digital camera (Canon PowerShot G10) controlled by Computer 2 was used to take the photographs of the yarn structure at the initial state and stretched state. A photograph of the auxetic plied yarn structure was taken at every 3 seconds during the stretching process, which corresponded to a 1% interval of the axial strain $\varepsilon$. As shown in Figure 5, the photographs provided the maximal thickness of the auxetic plied yarn structure at the initial state $H_0$ and that at the stretched state H. The way was to first magnify all the photographs

with the same multiple and then measure the values of $H_0$ and H by counting the pixels. When $H_0$ and H were known, the radial strain $\varepsilon_r$ could be calculated from Equation (1).

$$\varepsilon_r = (H/H_0 - 1) * 100\% \quad (1)$$

As the axial strain $\varepsilon$ was directly provided by the tensile tester, the Poisson's ratio of the auxetic plied yarn structure $v$ was calculated using Equation (2).

$$v = - \varepsilon_r/\varepsilon \quad (2)$$

## 4. Geometrical analysis

### *4.1 Assumptions*

In order to theoretically predict the Poisson's ratio of the auxetic plied yarn structure for given axial strain $\varepsilon$, a geometrical analysis was conducted based on the following assumptions.

1) All the yarn components are assumed to be isotropic linear elastic materials with known Poisson's ratio values.
2) The extrusion and friction among the yarn components during the stretching process are ignored in the geometrical analysis.
3) The twists of the yarn structure are perfectly regular and a turn of the yarn structure can be used to represent the whole auxetic plied yarn structure.
4) All the yarn components always keep contacted in helical forms at both the initial state and stretched state. Their cross sections are assumed to be circular and keep circular when stretched.
5) The deformation process of the auxetic yarn structure can be divided into two stages. The first stage is defined from the initial state to the state where two stiff yarns fully move in the center of the yarn structure and just get in contact each other. In this stage, the main

deformation mode is the moving-in of the stiff yarns towards the center of the yarn structure with shape changes of the yarn components. As the stiff yarns are difficult to be extended under low loading condition, their diameter and length are assumed to be kept constant in this stage. However, the diameter and length of the soft yarns can be changed due to lower modulus. The second stage is defined from the beginning of contact of two stiff yarns to the breakage of the auxetic yarn structure. In this stage, the main deformation mode is the cross sectional contraction of all the yarn components due to high extension, and the diameter and length of the stiff yarns are no longer assumed to be constant.

### *4.2 Establishment of relationships among geometrical parameters*

Based on the above assumptions, the relationships among different geometrical parameters can be established. The side view and cross-section of the idealized auxetic plied yarn structure are shown in Figure 6 (a) and (b), respectively. For facilitating the geometrical analysis, the following parameters are firstly selected. They are: 1) diameter of stiff yarn $d$ and diameter of soft yarn D; 2) maximal thickness of the auxetic composite yarn structure H; 3) helical angle of stiff yarn $\theta_d$ and helical angle of soft yarn $\theta_D$; 4) length of the auxetic composite yarn structure in one turn of yarn L; 5) length of stiff yarn $S_d$ and length of soft yarn $S_D$ in one turn of the auxetic yarn structure; 6) distance between the cross sectional central points of the auxetic yarn structure O and stiff yarn $O_1$ $x_d$; 7) distance between the cross sectional central points of the auxetic yarn O and soft yarn $O_2$ $y_D$. The following geometrical analysis will establish the relationships of these parameters.

The relationship of H with other parameters will be first established from the cross sectional geometry of the auxetic plied yarn structure. As shown in Figure 6(b), two stiff yarns are located in two sides of two soft yarns and closely contact with them. As the cross section of

the auxetic plied yarn structure is not perpendicular to the axes of the stiff and soft yarns, both the cut stiff yarn and soft yarn cross sections are not circular, but in elliptical shapes. In order to facilitate the analysis, a coordinate system is firstly set-up with the original point O (0, 0) at the central point of the cross section of the auxetic plied yarn structure. The central point of the stiff yarn located at the left side and that of the soft yarn located at the lower side are $O_1$ ($-x_d$, 0) and $O_2$ (0, $-y_D$), respectively. The stiff yarn and soft yarn contact at point A ($x_0$, $y_0$) and their common tangent line passing by point A can be described by a linear equation $y = kx + b$, where $k$ is the slope and $b$ is the intercept. It is should be pointed out that H may not just be the distance between two extreme points $X_1$-$X_2$ in the x direction or $Y_1$-$Y_2$ in the y direction depending on diameter ratio of the stiff yarn and soft yarn and their cross sectional shapes as well as the distance of the stiff yarn to the central point O. Therefore, H should be defined as twice of the distance from the central point O to any point located on the surface of the stiff yarn $Q_1$ or soft yarn $Q_2$ which has a maximal distance to point O.

Introducing a parametric variable γ, any point on the surface of the stiff yarn $Q_1$ and that on the soft yarn $Q_2$ can be described by the following parametric equations for elliptical curves.

$$\text{At Q1, } x = -x_d + \frac{d}{2}\cos\gamma,\ y = \frac{d}{2\cos\theta_d}\sin\gamma;\ \text{at Q}_2,\ x = \frac{D}{2\cos\theta_D}\cos\gamma,\ y = -y_D + \frac{D}{2}\sin\gamma$$

$$(0 \le \gamma \le 2\pi) \qquad (3)$$

Therefore, the distance from point O to any point located on the surface of the stiff yarn $S_1$ and the distance from point O to any point located on the surface of the soft yarn $S_2$ can be calculated from Equation group (4).

$$\begin{cases} S_1 = \sqrt{\left(-x_d + \frac{d}{2}\cos\gamma\right)^2 + \left(\frac{d\sin\gamma}{2\cos\theta_d}\right)^2} \\ S_2 = \sqrt{\left(\frac{D\cos\gamma}{2\cos\theta_D}\right)^2 + \left(-y_D + \frac{D}{2}\sin\gamma\right)^2} \end{cases} \quad (0 \le \gamma \le 2\pi) \qquad (4)$$

From here, H can be determined by selecting a maximum value as defined by Equation (5).

$$H = 2*\text{Maximize}\ (S_1, S_2) \qquad (0 \le \gamma \le 2\pi) \tag{5}$$

Equation (4) and Equation (5) show that H has a relationship with parameters $d$, D, $\theta_d$, $\theta_D$, $x_d$ and $y_D$. These parameters are not independent and the relationships exist among them. As mentioned above, $y = kx + b$ is the common tangent equation of both the stiff and soft yarns at their contact point A which is also their tangent point. Based on the necessary and sufficient conditions of tangency between the stiff yarn and soft yarn, Equation group (6) can be obtained.

$$\begin{cases} y_0 = kx_0 + b \\ \frac{4(x_0+x_d)^2}{d^2} + \frac{4{y_0}^2}{d^2/\cos^2\theta_d} = 1 \\ \frac{4{x_0}^2}{D^2/\cos^2\theta_D} + \frac{4(y_0+y_D)^2}{D^2} = 1 \\ d^2 - 4b^2\cos^2\theta_d + d^2k^2\cos^2\theta_d + 8bkx_d\cos^2\theta_d - 4k^2{x_d}^2\cos^2\theta_d = 0 \\ D^2k^2 - 4b^2\cos^2\theta_D + D^2\cos^2\theta_D - 8by_D\cos^2\theta_D - 4{y_D}^2\cos^2\theta_D = 0 \end{cases} \tag{6}$$

Equation group (6) defines the relationships of parameters $d$, D, $\theta_d$, $\theta_D$, $x_d$ and $y_D$. As all the yarn components are twisted together in a helical form, other relationships can also be obtained by unfolding the helical stiff yarn and soft yarn into straight lines. Figure 7 shows the unfolded lines of both the stiff yarn and soft yarn in one turn of the auxetic plied yarn structure. They are just the inclination sides of the right triangles. From Figure 7, the following relationships are found.

$$S_d = L/\cos\theta_d \tag{7}$$

$$S_D = L/\cos\theta_D \tag{8}$$

$$x_d = L\tan\theta_d/(2\pi) \tag{9}$$

$$y_D = L\tan\theta_D/(2\pi) \tag{10}$$

### *4.3 Calculation of radial strain and Poisson's ratio*

Based on the above established relationships, the cross sectional deformation, i.e., radial strain $\varepsilon_r$, and Poisson's ratio $v$ of the auxetic plied yarn structure for any given axial strain $\varepsilon$ can be calculated from known parameters at the initial state. To avoid the confusion, the values of parameters L, $d$, D, $\theta_d$, $\theta_D$, $x_d$, $y_D$, $S_d$ and $S_D$ at the initial state are represented by $L_0$, $d_0$, $D_0$, $\theta_{d_0}$, $\theta_{D_0}$, $x_{d_0}$, $y_{D_0}$, $S_{d_0}$ and $S_{D_0}$. Analyzing the structural feature of the auxetic plied yarn structure, it is found that its geometry at the initial state can be determined by the following four independent parameters: diameter of the stiff yarn $d_0$ and diameter of the soft yarn $D_0$, twist of the auxetic plied yarn structure T and helical angle of the stiff yarn $\theta_{d_0}$. Since the axial strain $\varepsilon$ is given, according to Equation (1) and Equation (2), the calculation of $\varepsilon_r$ and $v$ consists in calculating $H_0$ and H from known parameters $d_0$, $D_0$, $\theta_{d_0}$ and T.

In addition to $d_0$, $D_0$, $\theta_{d_0}$ and T, other parameters at the initial state, including $L_0$, $\theta_{D_0}$, $x_{d_0}$, $y_{D_0}$, $S_{d_0}$, $S_{D_0}$ and $H_0$, also need to be determined for the subsequent calculations. Based on the helical form of the auxetic plied yarn structure, $L_0$ (mm) can be first calculated from T (turns/m) using Equation (11).

$$L_0 = 1000/T \tag{11}$$

When $L_0$ and $\theta_{D_0}$ are known, $S_{d_0}$, $S_{D_0}$ and $x_{d_0}$ can be calculated from Equation (7) to Equation (9), respectively. When $d_0$, $D_0$, $\theta_{D_0}$ and $x_{d_0}$ are known, $y_{D_0}$ and $\theta_{D_0}$ can be calculated by solving Equation group (6) and Equation (10). Therefore, the maximal thickness of the auxetic plied yarn structure in the initial state $H_0$ can be determined from Equation (5). The above steps for determining $H_0$ at the initial state is schematically shown in Figure 8.

According to Assumption 5, the deformation process of the yarn structure can be divided into two stages. The first stage is defined from the initial state to the state where two stiff yarns fully move in the center of the yarn structure and just get in contact each other, i.e., $\varepsilon$ changes from 0 to $\varepsilon_c$ where $\varepsilon_c$ is the critical axial strain at the end of the first stage. In the first stage, the diameter and length of the stiff yarn are assumed to be constant due to higher modulus than that of soft yarn, i.e., $d = d_0$, $S_d = S_{d_0}$. From $S_d = S_{d_0}$, Equation (12) can be obtained.

$$L/\cos\theta_d = L_0/\cos\theta_{d_0} \tag{12}$$

When the auxetic plied yarn structure is stretched to a given $\varepsilon$, its length in one turn of yarn $L_0$ also changes to L. The relationship of L and $L_0$ is given by Equation (13)

$$L = L_0(1+\varepsilon) \tag{13}$$

At the end of the first stage, $x_d = d_0/2$. Based on this condition, $\varepsilon_c$ can be determined from Equation (9), Equation (12) and Equation (13), and is given by Equation (14).

$$\varepsilon_{c=}\sqrt{\frac{1}{\cos^2\theta_{d_0}}-\frac{\pi^2{d_0}^2}{{L_0}^2}}-1 \tag{14}$$

In the first stage, although the diameter and the length of the stiff yarn in a turn of the auxetic yarn are assumed to be kept unchanged, the same assumption is not applied to the soft yarn due to their low modulus. As the soft yarn is assumed to be isotropic linear elastic material, its diameter D in the stretched state can be calculated from its Poisson's ratio $\nu_D$ by Equation (14).

$$D = D_0\left(1-\frac{S_D-S_{D_0}}{S_{D_0}}\nu_D\right) \tag{15}$$

From Equation (12) and Equation (13), $\theta_d$ can be determined for given $\varepsilon$. When $\theta_d$ is known, $x_d$ can be determined from Equation (9). When $d$, $\theta_d$ and $x_d$ are known, D, $\theta_D$ and $y_D$ can be

calculated by solving Equation group (6), Equation (10) and Equation (15). Therefore, H for given $\varepsilon$ in the first stage can be calculated from Equation (5). The above steps for determining H in the first stage is schematically shown in Figure 9.

The second stage is defined from the beginning of contact of the two stiff yarns to the breakage of the auxetic yarn structure. In this stage, although two stiff yarns always maintain to be contacted, that is, $x_d = d/2$, their cross section and length are no longer assumed to be constant. As the stiff yarn is assumed to be isotropic linear elastic material, its diameter $d$ in the second stage can be calculated from its Poisson's ratio $\nu_d$ by Equation (16).

$$d = d_0\left(1 - \frac{S_d - S_{d_0}}{S_{d_0}}\nu_d\right) \tag{16}$$

By solving Equation group (6), Equation (7), Equation (8), Equation (9), Equation (10), Equation (15) and Equation (16), $d$, D, $\theta_d$, $\theta_D$, $x_d$, $y_D$, $S_d$ and $S_D$ can be obtained. Therefore, H for given $\varepsilon$ bigger than $\varepsilon_c$ in the second stage can be determined from Equation (5). The above steps for determining H in the second stage is schematically shown in Figure 10.

## 5. Results and discussion

### *5.1 Variation of radial strain*

In order to understand the deformation behavior of the novel auxetic plied yarn structure under axial extension, Sample A1 is firstly chosen as an example to show how its cross section changes when stretched in the axial direction. The photographs of the yarn structure stretched at different axial strains and the curve of its radial stain as a function of axial strain are shown in Figure 11 and Figure 12, respectively. It can be seen that both the stiff and soft yarns are uniformly formed in a helical form in the initial state (Figure 11(a)). Under the axial extension, both the stiff and soft yarns will be deformed. At a low axial strain less than 0.10 (Figure 11(b)), the main deformation mode of the auxetic yarn structure is the shape change

of its yarn components with the movement of the stiff yarns towards the center of the auxetic plied yarn structure. As the moving-in of the stiff yarns pushes the soft yarns out, the cross-section of the auxetic composite yarn structure is increased. As a result, the radial strain of the yarn structure is rapidly increased to its maximal value as shown in Figure 12. After the axial strain exceeds about 0.10, although the helical angle of the stiff yarns continues to slowly decrease (Figure 11 (c) and (d)), the cross sectional contraction becomes the main deformation mode of both the stiff and soft yarns due to high axial extension, which results in a radial strain decrease of the auxetic plied yarn structure as shown in Figure 12. The auxtic plied yarn structure is destroyed when the stiff yarns are broken at a strain of 0.36 (Figure 11 (e)). The testing results confirm the two-stage deformation process of the auxetic plied yarn structure as assumed above.

The radial strain curve calculated from the known parameters of sample A1 at the initial state as listed in Table 1 (T = 52.63 turens/meter, $d_0$ = 0.78 mm, $D_0$ = 0.2.24 mm, $\theta_{d_0}$ = 18.52 degree) and the given Poisson's value of both soft yarn and stiff yarn ($\nu_d = \nu_D = 0.30$) is also shown in Figure 12 for comparison. While the calculation of $H_0$ follows the flow chart shown in Figure 8, the calculations of H in the first and second stages follow the flow charts shown in Figure 9 and Figure 10, respectively. After $H_0$ and H have been known, the radial strain $\varepsilon_r$ is calculated from Equation (1). It can be seen that both the experimental and calculated curves have the same variation trend, that is, the radial strain first increases and then decreases with the increase of the axial strain. Although some differences exist between the experimental and calculated results, the results from the geometrical analysis can well predict the axial deformation behavior of the auxetic plied yarn structure.

***5.2 Poisson's ratio***

The curves of Poisson's ratio as a function of the axial strain obtained from the experiment and calculation for four kinds of auxetic yarn samples are shown in Figure 13. It can be found that the Poisson's ratio values of all four samples are negative. These results confirm that the proposed plied yarn structure has auxetic effect. From Figure 13, it can be also found that the calculated results from the geometric analysis are close to the experiment ones, except in the initial extension stage where the variation trends between the experiment and calculation are opposite. Taking sample A1 again as one example, although the radial strain curve calculated has the same variation trend with that of the experiment as shown in Figure 12, the values of radial strain calculated are much higher than these from the experiment in the initial extension stage. As a result, the absolute Poisson's ratio values calculated in the initial extension stage are much higher than those from the experiment. The reason may originate from yarn slippage effect taking place between the stiff yarns and soft yarns in the initial extension stage, which results in higher axial strains of the auxetic yarn structure in the experiment. As the yarn slippage effect could not be taken in consideration in the geometrical analysis, the axial strains of the auxetic yarn structure calculated are lower than those from the experiment. Since the geometric analysis cannot well predict the Poisson's ratio of the auxetic yarn structure in the initial extension stage, a mechanical analysis by considering the yarn slippage effect is required. Such a kind of study is being carried out and the results will be published in our next paper.

## 6. Conclusions

A novel kind of plied yarn structure with NPR behavior was proposed and its deformation mechanism was presented. Four kinds of yarn samples were fabricated with two kinds of stiff yarns and two kinks of soft yarns, and tested under axial extension condition. A geometrical analysis was conducted and compared with the experiment. Based on both the experimental and geometrical analyses, the following conclusions are obtained.

1) The novel auxtic plied yarn structure has obvious NPR effect under the axial extension. However, the auxetic effect is varied with axial strain.
2) Although the geometric analysis can well predict the variation trend of the axial strain, it cannot well predict the Poisson's ratio of the auxetic yarn structure in the initial extension stage due to yarn slippage effect. Therefore, a mechanical analysis by considering the yarn slippage effect is required.

## Acknowledgement

The authors would like to acknowledge the funding support from the Research Grants Council of HK Special Administrative Region Government (Grant No. 515713).

## References

Alderson, A., Alderson, K. (2005). Expanding Materials and Applications: Exploiting Auxetic Textiles. *Technical Textiles International*, *14*(6), 29-34.

Alderson, K., Alderson, A., Anand, S., Simkins, V., Nazare, S., & Ravirala, N.(2012). Auxetic Warp Knit Textile Structures. *Physica Status Solidi(b)*, *249*(7), 1322-1329.

Alderson, K., Alderson, A., Smart, G., Simkins, V., & Davies, P. (2002). Auxetic polypropylene fibres: Part 1-Manufacture and characterisation. *Plastics, Rubber and Composites*, *31*(8), 344–349.

Alderson, K., Evans, K. (1992). The fabrication of microporous polyethylene having a negative Poisson's ratio. *Polymer*, 33(20), 4435–4438.

Alderson, A., Rasburn, J., Ameer-Beg, S., Mullarkey, Peter G., Perrie, W., and Evans, Kenneth E. (2000). An Auxetic Filter: A Tuneable Filter Displaying Enhanced Size

Selectivity or Defouling Properties. *Industrial Engineering Chemistry Research*, 39, 654-665.

Bhattacharya, S., Zhang, G., Ghita, O., & Evans, K. (2014). The variation in Poisson's ratio caused by interactions between core and wrap in helical composite auxetic yarns. *Composites Science and Technology*, 102, 87-93.

Chan, N., & Evans K. (1997). Fabrication methods for auxetic foams. *Journal of Materials Science*, 32(22), 5945–5953.

Evans, K., Donoghue, J., & Alderson, K. (2004). The design, matching and manufacture of auxetic carbon fibre laminates. *Journal of Composite Materials*, 38(2), 95–106.

Evans, K., Sloan, M., Wright, J., & Burns, M. (2010). Auxetic material. Patent, WO 2010146347.

Ge, Z., & Hu, H. (2013). Innovative three-dimensional fabric structure with negative Poisson's ratio for composite reinforcement. *Textile Research Journal*, 83(5), 543-550.

Ge, Z., Hu, H., & Liu, Y. (2013). A finite element analysis of a 3D auxetic textile structure for composite reinforcement. *Smart Materials and Structures*, 22(8), 084005.

Grima, J., Gatt, R., Zammit, V., Williams, J., Alderson, A., & Walton R. (2007). Natrolite: A zeolite with negative Poisson's ratios. *Journal of Applied Physics*, 101(8), 86102–086102–3.

Gunton, D., & Saunders, G. (1972). The Young's modulus and Poisson's ratio of arsenic, antimony and bismuth. *Journal of Materials Science*, 7(9), 1061–1068.

Hook, P. (2011). Uses of auxetic fibers. Patent, WO 2010146347.

Hook, P. (2009). Composite Fibre and Related Detection System, Patent, WO2007125352.

Hu, H., Wang, Z., & Liu, S. (2011). Development of Auxetic Fabrics Using Flat Knitting Technology. *Textile Research Journal*, 81(14), 1493-1502.

Hu, H., & Liu S. (2013). An auxetic yarn structure and relevant manufacturing method. Patent, CN 2012102128443.

Lakes, R. (1987). Foam structures with a negative Poisson's ratio. *Science*, 235, 1038–1040.

Lee, W., Lee S., Koh, C., & Heo, J. (2011). Moisture sensitive auxetic material. Patent, US 20110039088 A1.

Lees, C., Vincent, J., & Hillerton, J. (1991). Poisson's ratio in skin. *Bio-medical Materials and Engineering*, 1(1), 19–23.

Lim, T. (2014). Semi-auxetic yarns. *Physica Status Solidi (b)*, 251(2), 273-280.

Liu, Y., & Hu, H. (2010). A Review on Auxetic Structures and Polymeric Materials. *Scientific Research and Essays*, 5(10), 1052–1063.

Liu, Y., Hu, H., Lam J., & Liu, S. (2010). Negative Poisson's Ratio Weft-knitted Fabrics. *Textile Research Journal*, 80(9), 856-863.

Masters, I., & Evans, K. (1996). Models for the elastic deformation of honeycombs. *Composite Structures*, 35(4): 403–422.

Miller, W., Hook, P., Smith, C., Wang, X., & Evans, K. (2009). The manufacture and characterization of a novel, low modulus, negative Poisson's ratio composite. *Composites Science and Technology*, 69, 651–655.

Miller, W., Ren, Z., Smith, C., & Evans, K. (2012). A negative Poisson's ratio carbon fibre composite using a negative Poisson's ratio yarn reinforcement. *Composites Science and Technology*, 72, 761–766.

Ravirala, N., Alderson, K., Davies, P., Simkins, V., & Alderson, A. (2006). Negative Poisson's Ratio Polyester Fibers. *Textile Research Journal*, 76(7), 540–546.

Sloan, M., Wright J., & Evans, K. (2011). The helical auxetic yarn: a novel structure for composites and textiles–geometry, manufacture and mechanical properties. *Mechanics of Materials*, 43(9), 476–486.

Ugbolue, S., Kim, Y., Warner, S., Fan, Q., Yang, C., Olena, K., & Feng, Y. (2010). The formation and performance of auxetic textiles. Part I: theoretical and technical considerations. *Journal of the Textile Institute*, 101(7), 660-667.

Ugbolue S., Kim, Y., Warner, S., Fan, Q., Yang, C., Kyzymchuk, O., Feng, Y., & Lord, J. (2011). The formation and performance of auxetic textiles. Part II: geometry and structural properties. *Journal of the Textile Institute*, 102(5), 424–433.

Wang, Z., & Hu, H. (2014). Auxetic Materials and Their Potential Applications in Textiles. Textile Research Journal, 84(15), 1600–1611.

Wang, Z., & Hu, H. (2014). 3D Auxetic Warp-knitted Spacer Fabrics. Physica Status Solidi B, 251(2), 281–288.

Wang, Z., Hu, H., & Xiao, X. (2014). Deformation behaviors of 3D auxetic spacer fabrics. Textile Research Journal, 84(13), 17–28.

Wright, J., Burns, M., James, E., Sloan, M, & Evans, K. (2011). On the Design and Characterization of low-Stiffness Auxetic Yarns and Fabrics. Textile Research Journal, 82(7), 645-654.

Wright, J., Sloan, M., & Evans, K. (2010). Tensile properties of helical auxetic structures: A numerical study, Journal of Applied Physics, 108(4), 044905.

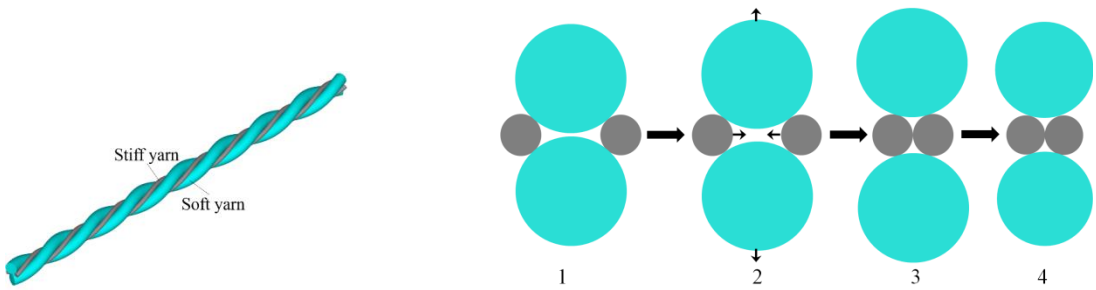


(a) (b)

Figure 1. Schematic illustration of the novel auxetic plied yarn structure: (a) side view; (b) cross section at different states

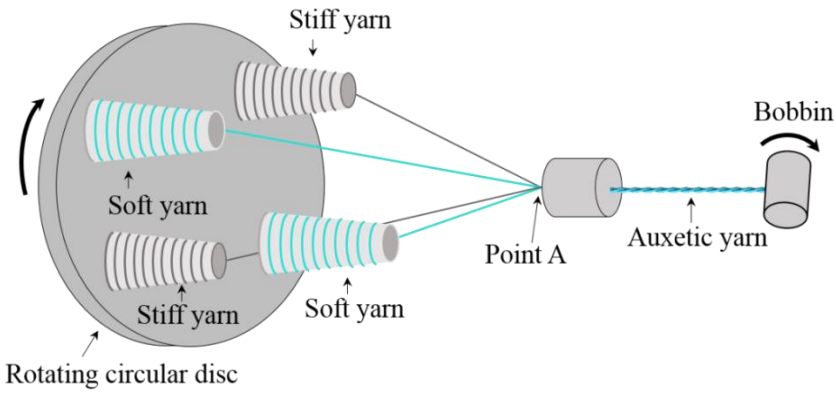


Figure 2. Manufacturing process of the novel auxetic yarn structure

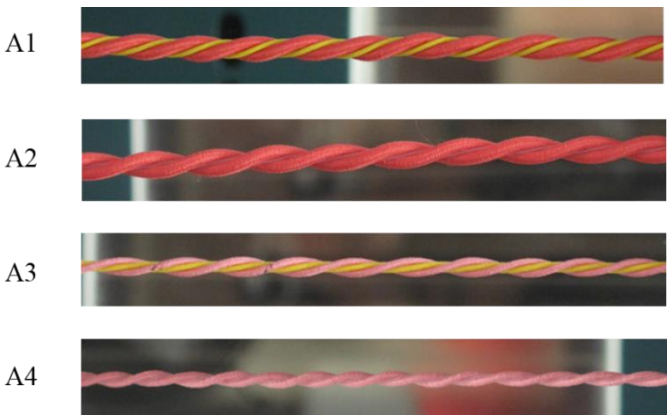


Figure 3. Photographs of the auxetic yarn samples fabricated

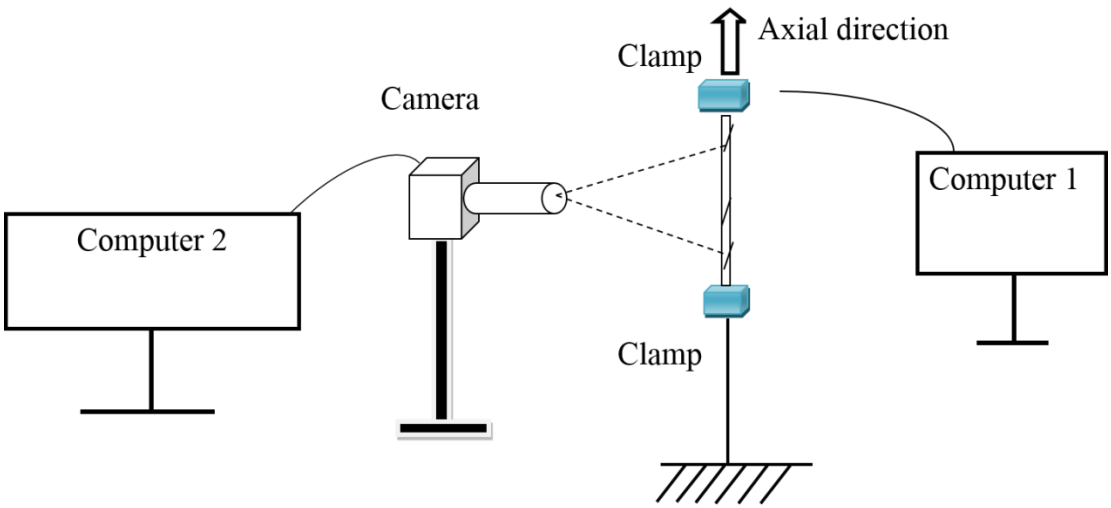


Figure 4. Set-up of testing system

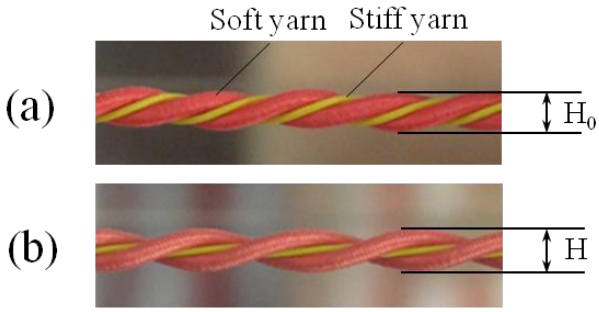


Figure 5. Photographs of the auxetic plied yarn structure at different states: (a) initial state; (b) stretched state

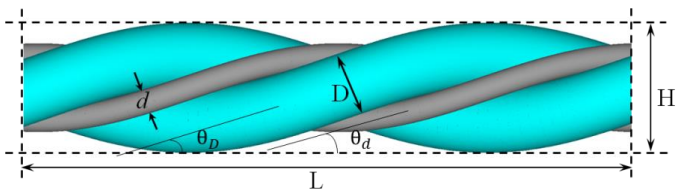


(a)

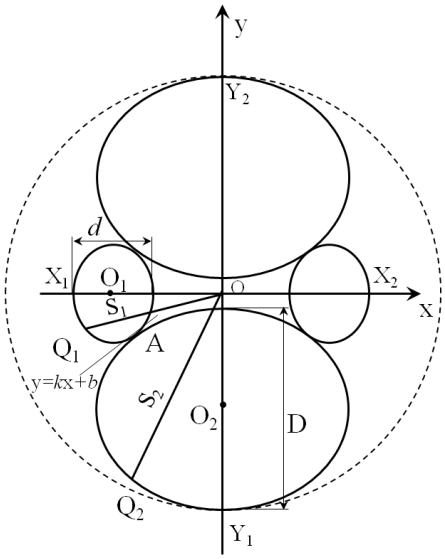


(b)

Figure 6. The idealized auxetic plied yarn structure: (a) side view; (b) cross section

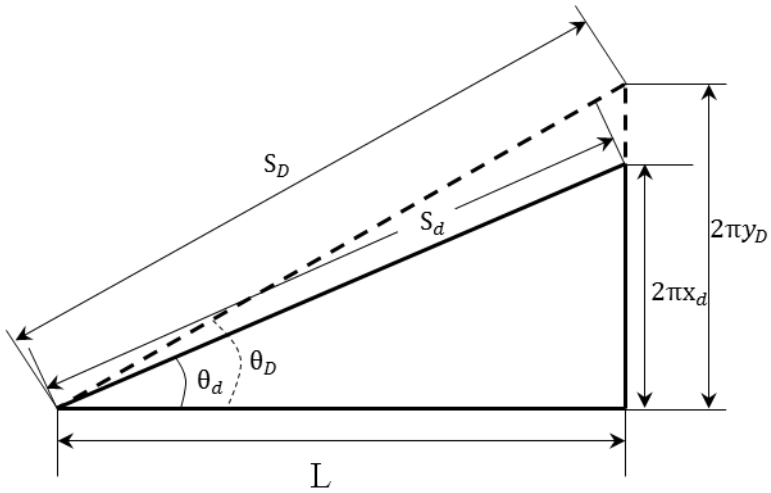


Figure 7. The unfolded lines of stiff and soft yarns in one turn of the auxetic yarn

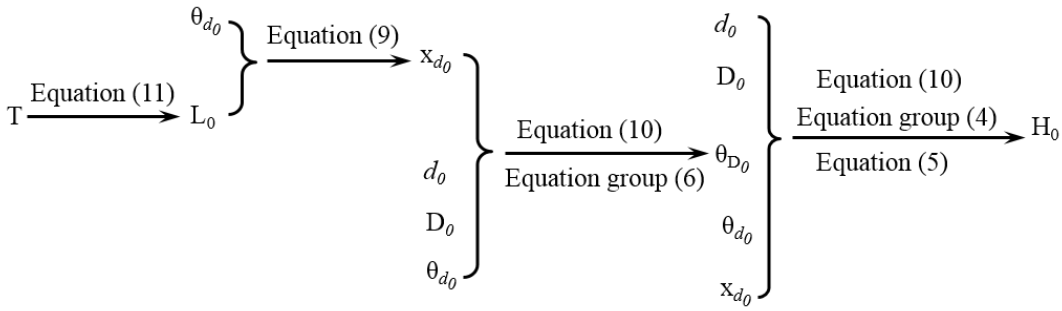


Figure 8. Flow chart for determining $H_0$ at the initial state

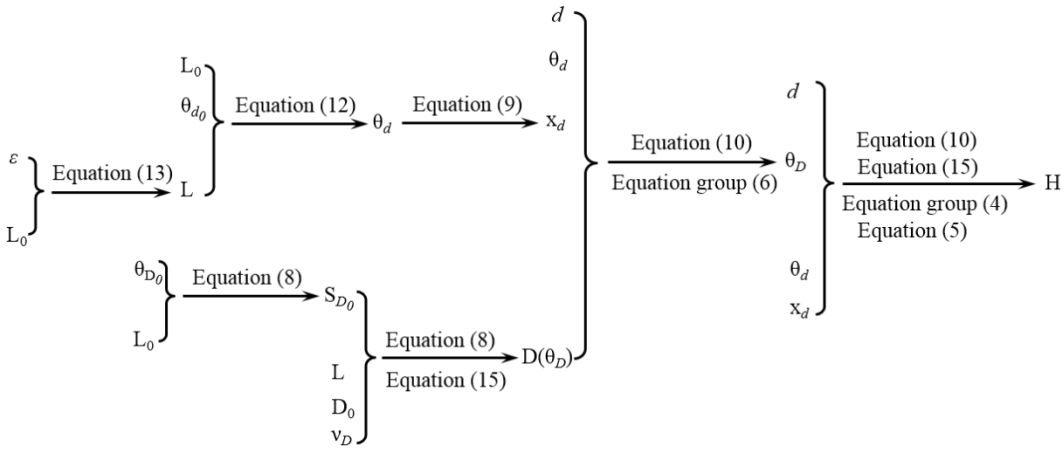


Note: $D(\theta_D)$ is a function of $\theta_D$

Figure 9. Flow chart for determining H in the first stage

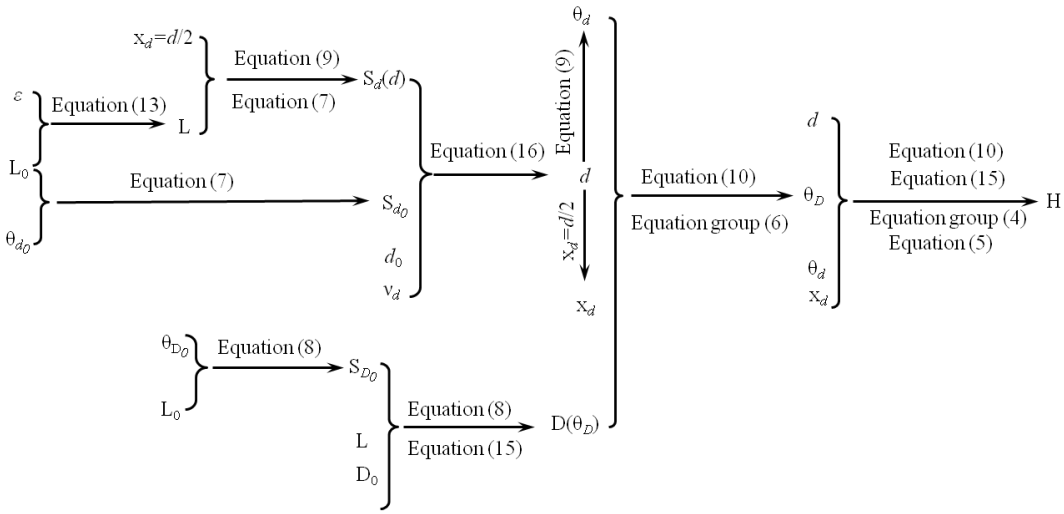


Notes: $S_d$ ($d$) is a function of $d$; $D(\theta_D)$ is a function of $\theta_D$

Figure 10. Flow chart for determining H in the second stage

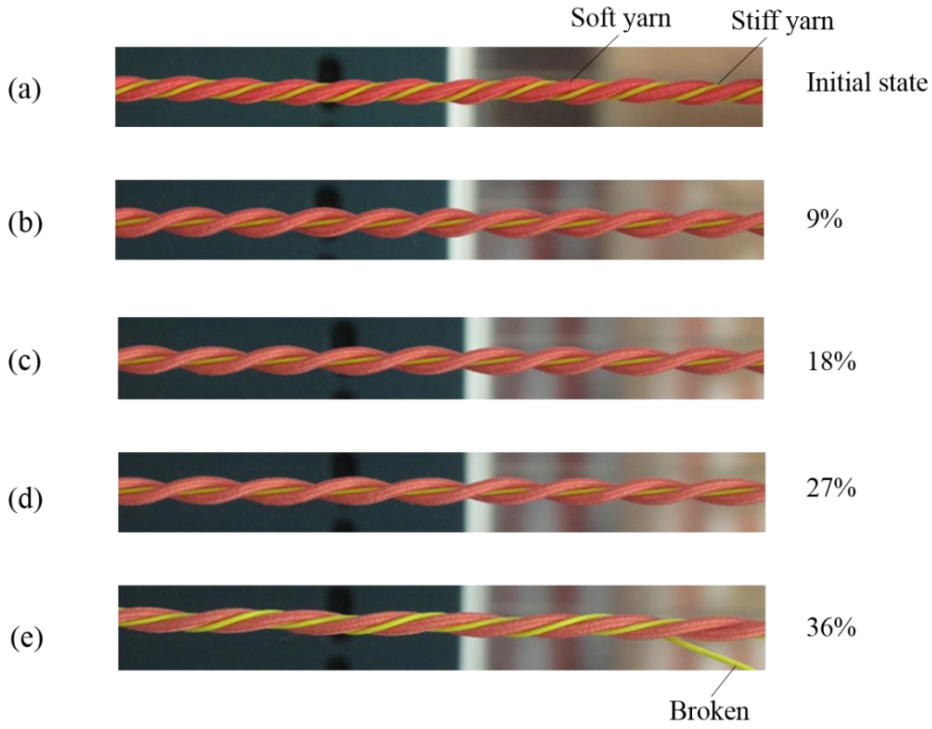


Figure 11. Photographs of Sample A1 stretched at different axial strains

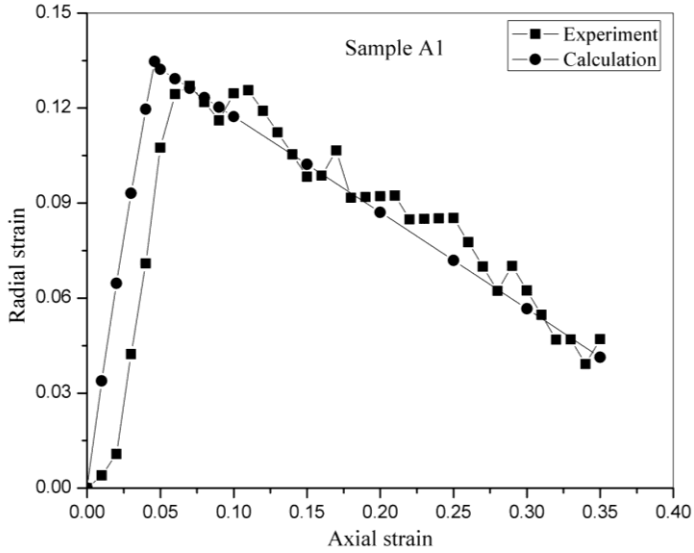


Figure 12. Radial strain as a function of axial strain for Sample A1

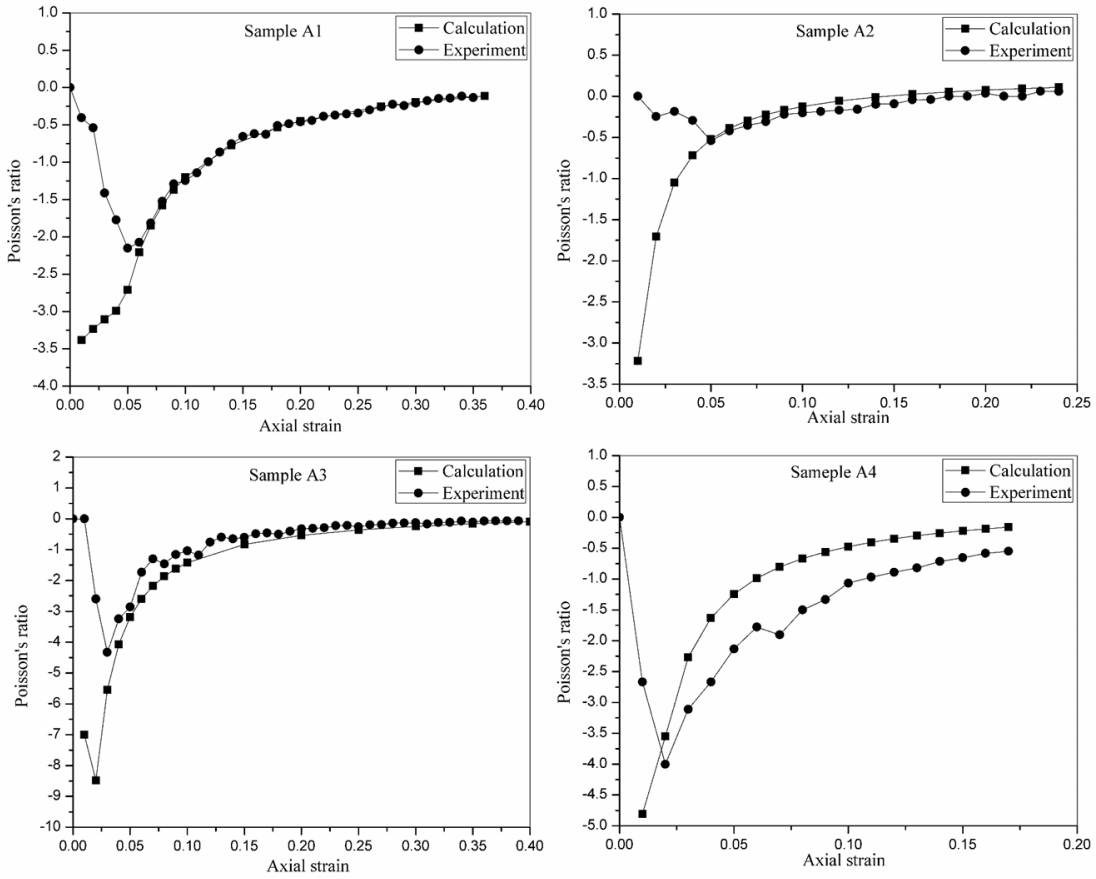


Figure 13. Poisson's ratio as a function of the axial strain

Table 1. Yarn components and structural parameters of the auxetic plied yarns

| Sample code | Yarn twist (turns/meter) | Stiff yarn | | | | Soft yarn | | |
|---|---|---|---|---|---|---|---|---|
| | | Material | Diameter (mm) | Elastic Modulus (MPa) | Helical angle (degree) | Material | Diameter (mm) | Elastic Modulus (MPa) |
| A1 | 52.63 | Polyester monofilament covered yarn | 0.78 | 1017.15 | 18.52 | Spandex covered yarn | 2.04 | 4.49 |
| A2 | 53.33 | Polyamide monofilament | 0.18 | 4178.07 | 8.78 | Spandex covered yarn | 2.04 | 4.49 |
| A3 | 50.71 | Polyester monofilament covered yarn | 0.78 | 1017.15 | 13.14 | Spandex covered yarn | 1.02 | 1.56 |
| A4 | 89.73 | Polyamide monofilament | 0.18 | 4178.07 | 10.42 | Spandex covered yarn | 1.02 | 1.56 |